Polymer Testing 92 (2020) 106866

Contents lists available at ScienceDirect

Polymer Testing

journal homepage: http://www.elsevier.com/locate/polytest

Measurement of the in-plane temperature field on the build plate during polymer extrusion additive manufacturing using infrared thermometry

Hardikkumar Prajapati, Swapnil S. Salvi, Darshan Ravoori, Ankur Jain *

Mechanical and Aerospace Engineering Department, University of Texas at Arlington, Arlington, TX, USA

ARTICLE INFO

Keywords:
Additive manufacturing
Polymer extrusion
Temperature measurement
Infrared thermography

ABSTRACT

The process of filament-to-filament adhesion during polymer extrusion additive manufacturing (AM) is critically influenced by temperature distribution around the filament. Direct measurement of temperature distribution around the filament being deposited is, therefore, important for fully understanding this critical process. While past papers have reported side-view (x-z) temperature measurement using infrared (IR) thermography, this paper presents measurement of the in-plane (x-y) temperature field on the build plate during printing of the first layer by infrared thermography. This measurement is carried out from under the build plate. A small part of the build plate is replaced by an infrared-transparent window. In conjunction with an infrared right-angle prism mirror positioned underneath, direct measurement of in-plane temperature distribution is carried out with an infrared camera. With a thin graphite coating on the build plate, in-plane temperature field on the build plate is obtained, whereas experiments without the graphite coating result in direct measurement of the filament temperature distribution. Bottom-view measurements are shown to agree well with side-view measurements. Temperature fields on the build plate are measured as functions of time for single-line and multi-line printing. A few key features revealed by measurements include symmetrical and asymmetrical temperature distributions for single and multi-line printing, respectively, and the thermal influence between lines being limited only to the adjacent line. The in-plane temperature measurement approach complements past side-view measurements, and improves upon our understanding of thermal phenomena during polymer AM.

1. Introduction

In several polymer-based additive manufacturing (AM) methods, a thermoplastic material heated up to a temperature exceeding the glass transition temperature is selectively rastered from a nozzle on to a platform bed [1–3]. This class of additive manufacturing techniques has been widely used for a number of engineering and biomedical applications [4,5]. While originally used only for printing of non-functional prototypes and models, polymer AM is now increasingly being investigated for printing functional components capable of bearing thermal and mechanical load [6].

Ensuring good thermal and mechanical properties of additively printed polymer parts is of critical importance [7,8]. Good adhesion between adjacent polymer filaments must be ensured during the printing process since poor filament-to-filament contact leads to deteriorated thermal and mechanical properties [8,9]. Similarly, good adhesion between the build plate and the first layer of filaments is also important to prevent warping or delamination [10]. The adhesion between the build plate and the first layer of filaments is strongly governed by the temperature field around the filament and on the build plate [11–14]. After the filament has been deposited, it is important to keep the interface temperature above glass transition temperature for as long as possible [15]. Measurement of temperature distribution during polymer AM, and particularly on the build plate during the printing of the first layer is, therefore, critically important.

A number of temperature measurement techniques have been used for characterizing polymer AM processes. Micro-thermocouples integrated within the platform bed have been used to determine local temperature during the printing process [16]. This approach provides temperature only at the thermocouple location. Infrared thermography has also been used widely in polymer AM processes [17–22]. Infrared thermometry is based on measurement of thermal radiance emanating from a surface of interest and determination of the temperature field through the known emissivity of the surface [23]. At the macro scale, infrared thermography has been used for process monitoring [21]. Temperature field measurement during large area additive

* Corresponding author. Mechanical and Aerospace Engineering Department, University of Texas at Arlington, 500 W First St, Rm 211, Arlington, TX, 76019, USA.
E-mail address: jaina@uta.edu (A. Jain).

https://doi.org/10.1016/j.polymertesting.2020.106866
Received 26 May 2020; Received in revised form 21 July 2020; Accepted 16 September 2020
Available online 19 September 2020

manufacturing of pyramid test structures using Acrylonitrile butadiene styrene (ABS) with 20% glass fiber has been presented [19]. An IR camera has been used to monitor the temperature at the exit of the liquefier [20]. Temperature distribution in the filament in the stand-off gap between the nozzle tip and platform bed has also been measured and compared against a conduction-advection thermal model [22]. A metal heater has been integrated with the filament nozzle to provide *in situ* heating from very close distance during the rastering process [24]. Infrared camera has been used for thermal imaging to correlate microwave exposure with dielectric measurements on the filament [25]. In a Big Area Additive Manufacturing (BAAM) system, IR pre-heating has been used to control the substrate temperature and temperature has been monitored using pyrometers mounted to the deposition head [26]. Mid- and long-wave infrared camera have been used to measure temperature of the printing layer for small-scale and BAAM printers [27]. In another study, infrared camera has been used to study the temperature profile of the interface under different nozzle temperature, platform temperature, printing speed and layer thickness [28]. Infrared camera has also been used while printing a standard tensile strength test sample to monitor the temperature distribution of the layers [29].

Infrared thermography has also been used at the microscale to investigate thermal processes after deposition. A side-view infrared camera has been used to determine temperature distribution in the *x*-*z* plane (see Fig. 1 for coordinate system), both for single-layer [17] and multi-layer printing [18]. These measurements provide temperature at the interface between filaments that are neighbors in the build direction (*z*). Through these measurements, temperature at the interface between filaments in neighboring layers and its evolution with time has been estimated.

In contrast to side-view measurement presented in these papers, there remains a lack of experimental measurement of in-plane temperature distribution on the build plate (*x*-*y*). Side-view measurements provide temperature distribution in the *x*-*z* plane, and therefore, specifically investigate adhesion between filaments in adjacent layers. On the other hand, adhesion between neighboring filaments on the same plane is also important, and this can be understood by measuring the in-plane temperature distribution. Unfortunately, there are several challenges in such a measurement. While a side view measurement can be carried out by mounting an infrared camera on the side of the 3D printer [17,18], measurement of the in-plane temperature is more challenging due to lack of optical access. Viewing from the top is not effective, because the moving nozzle assembly blocks the view of the key region of interest where the filament is being deposited. By the time the nozzle moves away and allows optical access to the overhead IR camera, thermal diffusion would be largely complete.

Given the importance of measuring the in-plane temperature field on the build plate (*xy*), this paper presents a technique for measurement of in-plane temperature distribution on the build plate from underneath. While viewing from the bottom does not offer thermal information related to printing of the second and subsequent layers, the information obtained on the interaction between the first layer and the print bed itself is important, as it may help understand filament-to-bed thermal interactions and stress development. The temperature field between the first layer and the bed has been shown to strongly impact the adhesion force [14]. Inadequate adhesion between the first layer and the build plate may lead to warping and deformation during the printing process. Therefore, measurement of temperature field around the first layer is important, for which, the bottom view approach is appropriate. Further, while past side view measurements help understand inter-layer bonding, the present work may help with understanding intra-layer bonding, i.e. bonding between in-plane neighbor filaments in the context of the first layer. When combined, the two distinct measurement approaches may provide a more comprehensive thermal picture of the polymer AM process.

2. Experimental setup

2.1. Additive manufacturing platform

The experimental setup is shown schematically in Fig. 1, with pictures shown in Fig. 2. An open source Anet A8 3D printer is used in this work. The platform bed comprises a 6.20 mm thick Aluminum plate, in which a small, 12.70 mm diameter through-hole with 3.20 mm step is drilled to provide optical access to the platform bed from the bottom. A 12.70 mm diameter IR-transparent Sapphire window is placed in the through-hole. ABS filament of black color and 1.75 mm diameter is used. The layer height is 0.4 mm and nozzle diameter is 0.4 mm. The nozzle is heated up to 230 °C. The print bed is maintained at 88 °C using a 3.8 Ω resistive heater comprising 20 BNC Nichrome wire folded into nine turns, sandwiched between Kapton tape and attached to the platform bed using adhesive. NTC 3950 100K Ohm thermistor is attached to the bed to monitor and control the bed temperature. It is verified through thermocouple measurements that the bed heater maintains the Sapphire window at the same initial temperature as the bed. Two layers of cardboard are provided on the back side of the bed for thermal insulation, with a through-hole provided for optical access. One layer of Kapton tape is applied on the top surface of the bed to improve adhesion to the dispensed filament. The bed is installed on the 3D printer and elevated using a threaded rod. The bed is leveled by adjusting the elevation at five points – four corners and center – such that a sheet of paper slides through with minimum resistance.

2.2. Infrared thermography setup and calibration

Fig. 2 presents a picture of the experimental setup, showing the build plate with an IR-transparent Sapphire window, an IR mirror directly underneath and an IR camera placed horizontally across the mirror. The optical path for the infrared signal is shown with a broken red line. The mirror used in this work is a right-angled gold coated infrared mirror. The FLIR A6703sc infrared camera used in this work operates in the

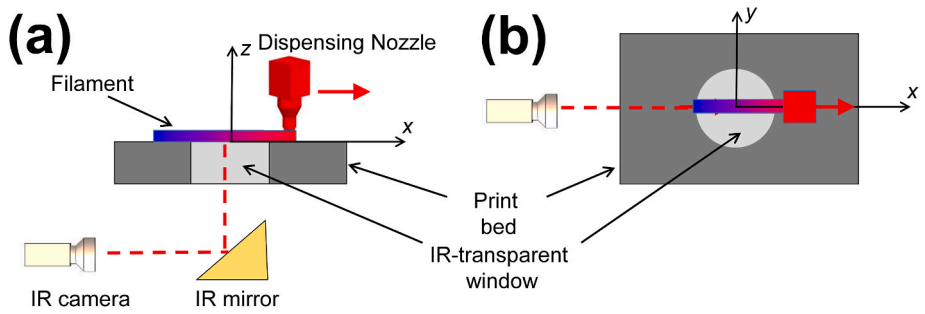

Fig. 1. Schematic of the experimental approach for bottom-view measurement of in-plane (*x*–*y*) temperature field on the print bed. (a) and (b) show side view and bottom view, respectively. Use of graphite layer on print bed facilitates measurement of in-plane temperature distribution, whereas filament temperature is measured when no graphite is present. Note that these schematics are not to scale.

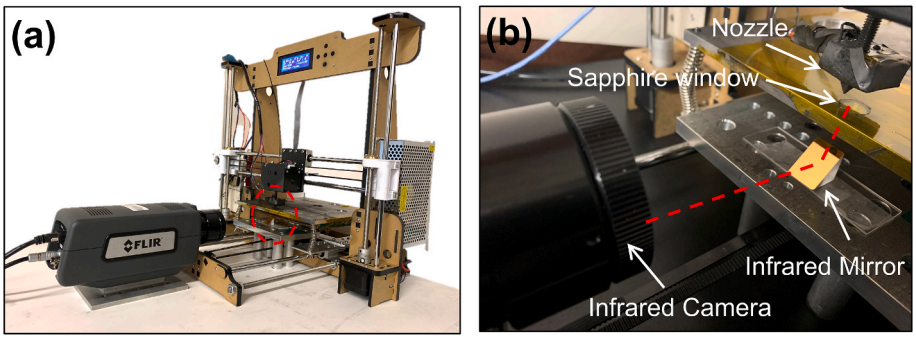

Fig. 2. Pictures of the experimental setup for measurement of in-plane temperature distribution on the print bed. (a) presents a picture of the overall experimental setup, and (b) presents a zoomed-in picture showing the IR-transparent window, IR mirror and IR camera lens. Optical path from the build plane to the IR camera is shown schematically with a broken line.

3.0–5.0 μm wavelength range with a spatial resolution of 37 μm and frame rate of 60 Hz. Experiments are carried out both with and without a thin (<1 μm) graphite layer sprayed on the build plate. Since graphite is opaque to infrared radiation, the presence of graphite enables measurement of temperature on the build plane. On the other hand, experiments without the graphite layer directly measure temperature of the filament above the build plane. Since the graphite is very thin, it has negligible thermal mass, and does not impact the temperature field itself.

Note that a key general limitation of the present approach of measuring temperature distribution from the bottom is that only temperature on the build plate is accessible. Therefore, the bottom-view measurement is limited to characterization of temperature field within the first layer, and its interactions with the build plate. Temperature distribution in further layers in case of multi-layer printing can not be determined due to the IR-opaque nature of filament material.

Calibration of the measured infrared signal is a critical process that affects the accuracy of temperature measurements. Since infrared emission passes through a complicated path including the IR-transparent window and IR mirror, it is important to carry out calibration in identical settings as the actual experiment. There are two possible approaches for calibration – infrared intensity could be measured at multiple known temperatures in order to create a look up table to be used to convert measured infrared intensity during actual experiments to temperature [18]. Alternately, the emissivity of the surface of interest could be determined such that there is best-possible agreement between a set of known temperatures and predicted temperatures corresponding to each [17]. In the present case, the latter approach is used due to good linearity observed in calibration data. In calibration experiments, the Instec HCS662V hot stage capable of being maintained at desired temperatures is placed on the platform bed in such a way that the stage and IR window are aligned. A K-type thermocouple is used to measure temperature of top surface of the stage. Measurements are carried out in 70–240 °C range, which covers the entire temperature range expected during actual experiments. Sufficient time is provided to reach steady state at each temperature, following which, the infrared intensity in measured. The hot stage is coated with the same graphite spray and covered with Kapton tape that are also used on the platform bed during actual experiments. Emissivity of the graphite film covered with Kapton tape is determined to be 0.806 by comparison of infrared-based temperature with thermocouple-based measurement over the entire temperature range of calibration. A separate calibration experiment is carried out with a pre-fabricated ABS sample when viewed through the Sapphire window and Kapton tape. The resulting emissivity value of 0.797 is used for experiments without graphite that directly measure the filament temperature. Calibration results are discussed in Section 3.6.

3. Results and discussion

Measured temperature fields in a variety of printing conditions are presented and discussed in this section. These experiments are carried out both with and without graphite layer. With a thin graphite coating on the build plate, in-plane temperature field on the build plane is obtained, whereas experiments without the graphite coating result in direct measurement of the filament temperature distribution. Data from both types of measurements are presented in Section 3.1-3.4. Further sub-sections discuss the role of the graphite layer and calibration measurements.

3.1. Thermal images

This section presents measured colormaps of temperature fields during the polymer AM process. Fig. 3 shows a succession of build plate temperature distribution at multiple times for single-line printing, where the nozzle rasters from left to right at 3600 mm/min speed. Emissivity calibration for graphite is used in Fig. 3. The circular, light-blue region in these images is the IR-transparent window on the build plate through which the imaging is carried out. The nozzle size is shown as a circle for comparison. These images clearly capture the temperature distribution in the *x-y* build plane, showing the motion of the peak temperature as the nozzle traverses from left to right. There is a significant temperature distribution behind the nozzle, with very little impact upstream. These are both consistent with results from moving heat source theory [17]. There is also a strong temperature gradient in the *y* direction. The zone of influence in the *y* direction is limited to around 2 mm.

In contrast with Fig. 3 that presents temperature distribution on the build plane, Fig. 4 presents thermal images without the IR-opaque graphite layer on the build plane. In this case, the IR camera directly measures temperature distribution on the filament. In addition to the filament, the nozzle itself is also visible as it moves from left to right. Filament temperatures reported in Fig. 4 are significantly greater than print bed temperatures in Fig. 3, as expected. Note that thermal images in Fig. 4 are calibrated based on separately-measured emissivity of ABS. As a result, the temperature field displayed in Fig. 4 for regions other than the ABS filament may not be quantitative.

For further demonstration of the capability to measure the in-plane temperature field on the print bed, Fig. 5(a)-(d) present similar succession of IR thermal maps for a case where the nozzle takes a U-turn to print the next line. The line-to-line gap is 0 μm in this case, and nozzle moves at 3600 mm/min. The U-turn taken by the nozzle is quite apparent by following the head of the temperature distribution in this case.

Finally, Fig. 6 illustrates a more complicated printing pattern, where the nozzle is programmed to follow a circular path. The corresponding circular nature of the temperature distribution can be seen clearly. Fig. 6

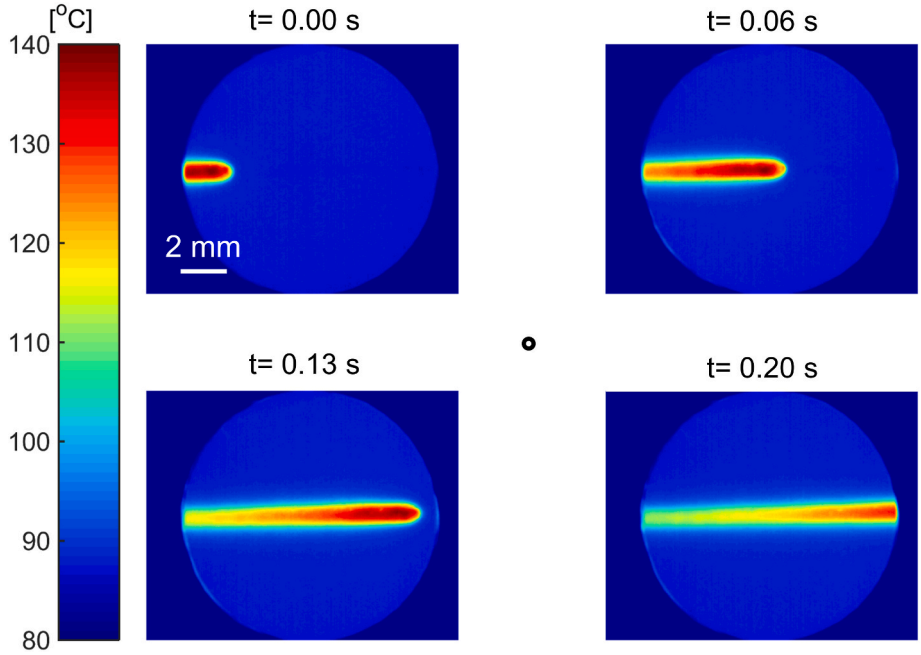

Fig. 3. Measured temperature distribution on the build plate at four different times during single-line dispense from left to right across the viewing window at 3600 mm/min raster speed. For reference, the circle in the center represents the nozzle size.

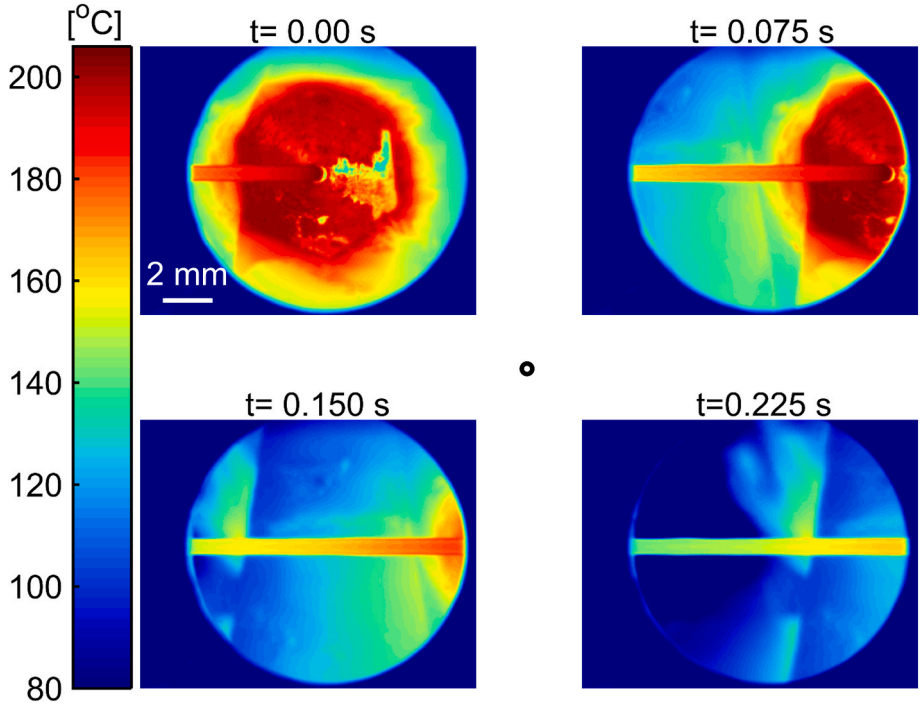

Fig. 4. Measured temperature distribution without graphite layer on the build plate, which facilitates measurement of filament temperature. Process conditions are identical to Fig. 3.

demonstrates the capability of bottom-view in-plane temperature field measurement even when the nozzle follows a geometry other than simply a straight line.

Each of the thermal images shown in Figs. 3–6 contain quantitative temperature data. Such data may be extracted from transient temperature colormaps for a quantitative understanding of heat transfer during the rastering process, as discussed in the next two sub-sections. Further, validation of the bottom-view measurements approach by comparison with filament temperature measurement from the side-view is discussed in Section 3.4.

3.2. Temperature distribution in x and y directions: single line printing

Fig. 7 plots print bed temperature as a function of y at a fixed location along the raster line at multiple times. Plots before and after $t = 0$, when the nozzle reaches the y axis are presented in Fig. 7(a) and (b), respectively. Fig. 7(a) shows a slow increase in temperature initially, followed by a rapid change as the nozzle approaches the y axis. There is some

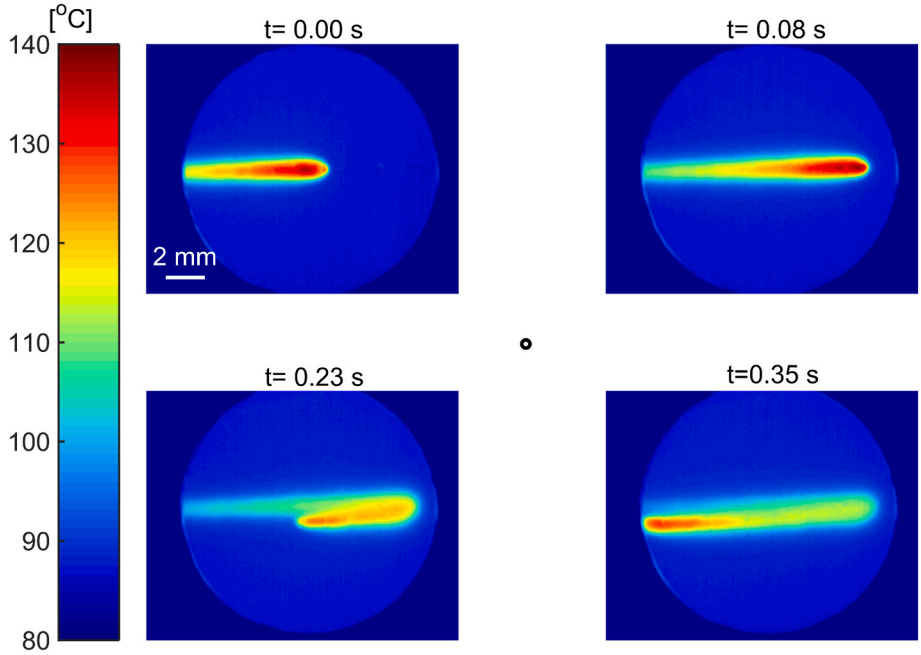

Fig. 5. Measured temperature distribution on the build plate at four different times during two-line dispense where the nozzle move from left to right across the viewing window at 3600 mm/min raster speed and then takes a U-turn to print the second line.

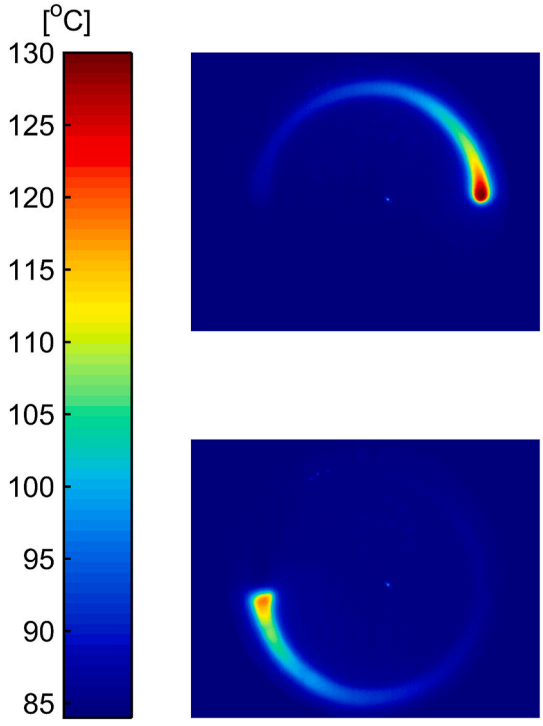

Fig. 6. Measured temperature distribution on the build plate at two different times during dispense in a circular path at 2500 mm/min.

upstream influence of the rastering nozzle as seen by temperature rise even before the nozzle reaches the y axis. Also note the very rapid rise in temperature along the y axis as the nozzle gets close. There is dramatic temperature rise between $t = -0.03$ s and $t = 0.00$ s.

The highest temperature is measured when the nozzle is directly above the y axis along the raster line. The thermal zone of influence is limited to around 2.0 mm around the raster line – beyond this zone, no thermal influence of the rastering process is observed. The region that experiences a temperature greater than the glass transition temperature is even narrower.

Temperature plots after the nozzle has crossed the y axis are shown in Fig. 7(b). These plots are characterized by a gradual drop in temperature, taking around 1.2 s for the peak temperature to drop below glass transition temperature. Within around 2.2 s, the thermal influence of the rastering process disappears completely.

While this study does not measure the temperature field for different filament sizes, it is expected, based on Fig. 7(a) and (b), that the thermal zone of influence may be a function of the filament size.

In each plot in Fig. 7(a) and (b), there is excellent symmetry in the measured temperature distribution about the x axis. This is expected since this is a single-line rastering experiment, and therefore, there is no influence from neighboring pre-deposited lines that might still be hot. Results from two-line rastering experiments are discussed in Section 3.3.

Plots of temperature distribution along the raster line are presented in Fig. 8(a) and (b). Plots prior to the nozzle reaching the y axis are presented in Fig. 8(a), while those afterwards are presented in Fig. 8(b). At any time prior to the nozzle reaching the y axis, there is strong upstream-downstream asymmetry, with a sharp, linear region behind the nozzle and sudden drop in temperature ahead of the nozzle. This is consistent with dominance of thermal advection over thermal diffusion, in this case, due to relatively large nozzle speed and low thermal diffusivity of the print bed. The location of the temperature peak moves, as expected, corresponding to nozzle motion from left to right. However, the peak temperature does not change appreciably over time behind the nozzle. The cooling down process along the x axis after the nozzle has passed is presented in Fig. 8(b), showing gradual reduction in temperature over time. Within around two seconds, the region plotted in Fig. 8 (b) completely cools down to the temperature of the print bed.

In conjunction with measurement of the in-plane temperature field on the build plate, temperature distribution on the filament surface is also measured as a function of time. Fig. 9 plots these data as a function of time, starting at $t = 0$ just after filament deposition. As expected, the temperature reduces with time over the entire filament surface. Fig. 9 shows that while there is some gradient in the temperature distribution across the filament, the filament temperature becomes more and more uniform as it decays with time.

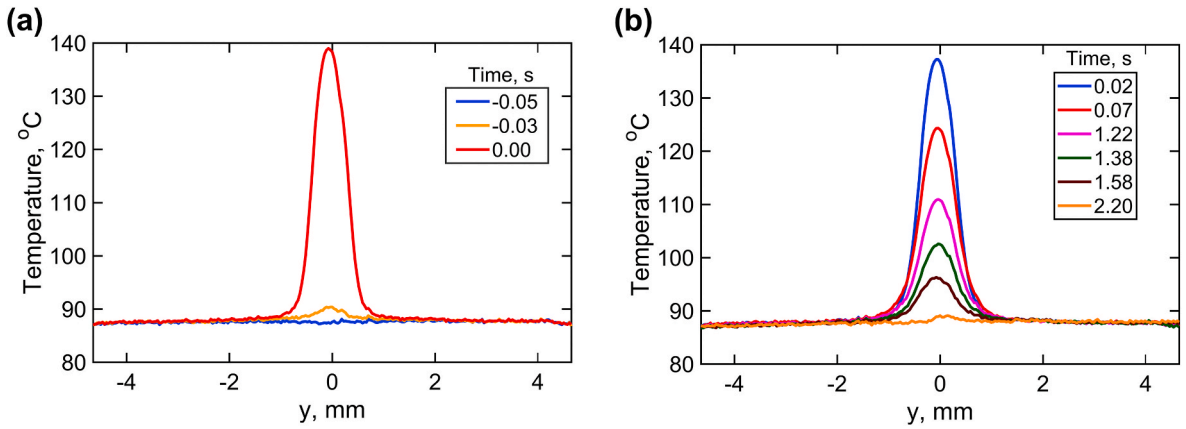

Fig. 7. Measured build plate temperature distribution in the y direction at multiple times during single-line rastering along the x axis at 3600 mm/min. (a) and (b) present plots at multiple times before and after nozzle passes over the y axis at $t = 0$.

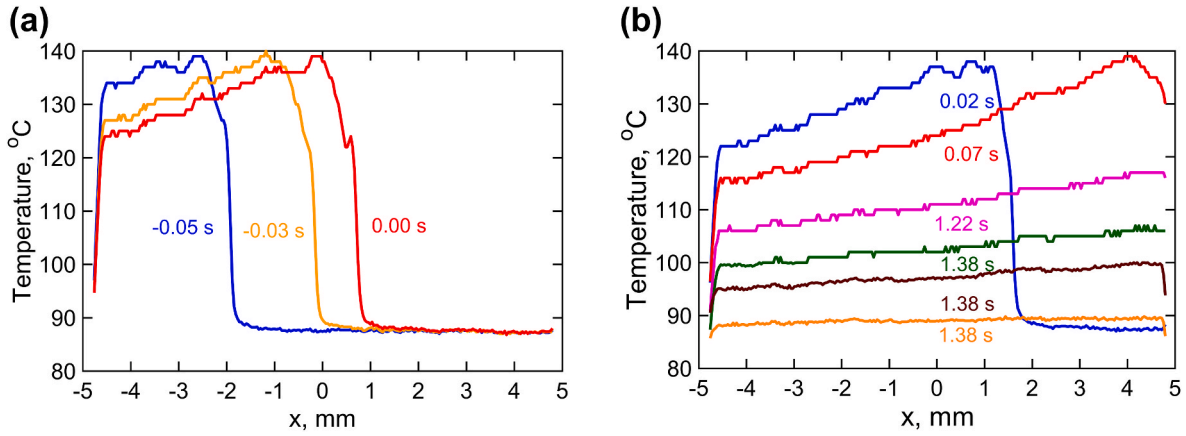

Fig. 8. Measured build plate temperature distribution in the x direction along the raster line at multiple times during single-line rastering along the x axis at 3600 mm/min. (a) and (b) present plots at multiple times before and after nozzle passes over the y axis at $t = 0$.

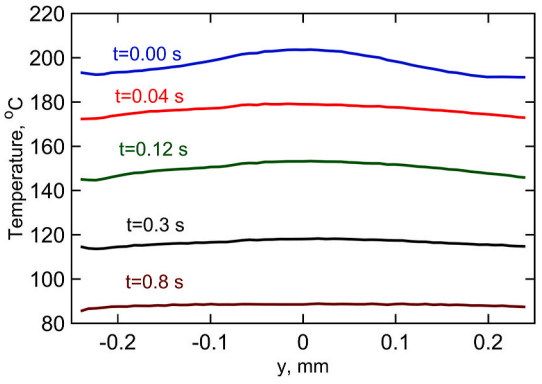

Fig. 9. Measured temperature distribution across the filament at multiple times, starting at deposition ($t = 0$).

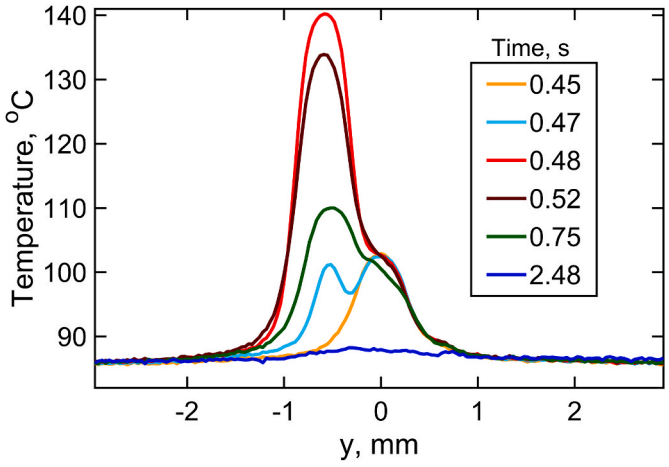

Fig. 10. Measured build plate temperature distribution in the y direction at multiple times during double-line rastering of 28 mm length at 3600 mm/min. The line-to-line gap is 0 μm.

3.3. *Temperature distribution in y direction: multi-line printing*

The previous sub-section discussed single-line rastering experiments that are shown to exhibit strong symmetry about the x axis in Fig. 7. Multi-line printing is an important process, as it may help understand filament-to-filament adhesion between in-plane neighbors. Measurements of temperature of filament-to-filament interface as well as the print bed during multi-line printing is discussed next.

Fig. 10 plots build plate temperature along the y axis for two-line printing, where the nozzle takes a U-turn at the end of the first line to dispense the second line with a gap of 0 μm between lines. The location $y = 0$ corresponds to the first raster line, whereas the second line is rastered at $y = -0.590$ mm. Data in Fig. 10 are presented at multiple times starting at $t = 0.45$ s, which corresponds to the nozzle reaching the

end of the first line. At this point, Fig. 10 shows a symmetric temperature distribution, as expected. Once the nozzle turns around and returns towards the y axis, a peak develops around $y = -0.590$ mm, corresponding to the second line. The temperature of the first raster line is still decaying, which results in a two-peak temperature distribution at $t = 0.47$ s. The peak corresponding to the first raster line is relatively smaller, and decays rapidly, so that by the time the temperature at the second line peaks at around $t = 0.48$ s, the thermal effect of the first line has nearly disappeared. Afterwards, the temperature distribution decays somewhat similar to Fig. 7(b), except for the peak having shifted to the location of the second raster line. The asymmetry in Fig. 10 represents an overlap of the heating up of the second line and cooling down of the first line, and is in contrast with the symmetric temperature curves for single-line printing shown in Fig. 7(a) and (b).

Temperature at the filament-to-filament interface is of specific interest because this temperature governs the extent and quality of bonding between the two filaments. Specifically, this interface must remain above glass transition temperature for as long as possible [13, 15]. Past papers have reported this critical temperature at the interface between neighboring filaments in the build (z) direction as a function of time. Similar to neighbors in the build direction, good bonding between in-plane neighbors is also critical for good properties of the built part. Using bottom-view measurement, Fig. 11 plots the measured interface temperature between filaments that are in-plane neighbors as a function of time. This experiment is carried out without graphite in order to directly measure the filament temperature. These curves are plotted for three different values of the filament-to-filament gap. As expected, the interface temperature is the highest – and decays at the lowest rate – when the filaments are closest to each other, at a 0 μm gap. The rate of decay is larger for the other two gaps investigated here. Considering the glass transition temperature of 106 °C for ABS, the interface for the 0 μm case remains above glass transition for around 0.25 s. Fig. 11 also shows an even shorter time above glass transition when the filament-to-filament gap is greater than 0 μm. The measured time above glass transition, even for the 0 μm gap case, is lower than reported by Seppala and Migler [18]. This is likely due to several reasons – firstly, Seppala and Migler reported this for neighboring filaments in the build direction, whereas the present work investigates in-plane neighbors. In their case, the recently printed, underlying layers may have been warm, whereas in the present case, the underlying layer is the print bed itself. Further, the print bed was set at 110 °C by Seppala & Migler, whereas it is set at 88 °C in the present work.

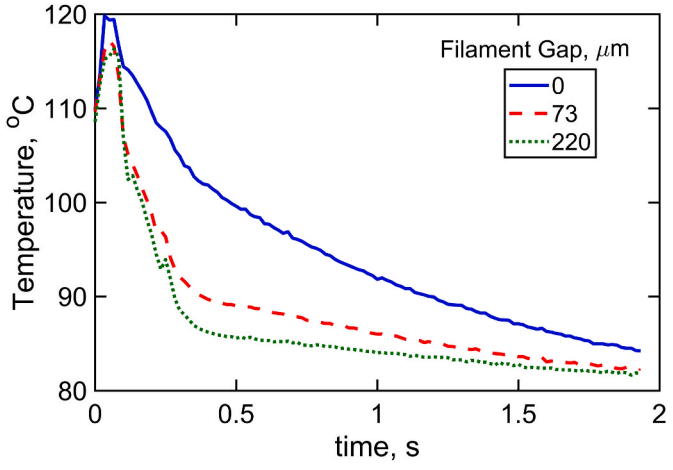

Fig. 11. Measured temperature of the interface between in-plane neighboring filaments as a function of time for three different filament-to-filament gaps.

3.4. Validation of bottom-view measurement by comparison with side-view measurement

In the absence of graphite coating on the print bed, the bottom-view approach facilitates measurement of the filament temperature and its evolution with time, such as shown in Fig. 4. It is of interest to compare such measurements against side-view measurements in order to validate the bottom-view measurement approach. To do so, temperature as a function of time at a specific point on the filament is extracted from the bottom-view measurement shown in Fig. 4. The printing process is repeated with the same process parameters, but with the infrared camera positioned sideways in order to measure the filament temperature from the side. Fig. 12 compares temperature as a function of time at a point on the filament measured with the bottom-view and side-view approaches. There is good agreement between the two independent approaches for filament temperature measurement, with both curves decaying at roughly the same rate.

3.5. The role of the graphite layer

The presence or absence of the graphite layer plays a key role in the measurements described here. Due to its IR-opaque nature, when sprayed on the print bed, it enables the infrared camera to measure the temperature field on the build plate. In the absence of the graphite layer, the infrared camera sees beyond the print bed, and with emissivity calibration for ABS, measures the temperature distribution on the filament. In order to illustrate the key role of the graphite layer, experiments are carried out with only the left half of the Sapphire window sprayed with graphite. In such a case, the left half measures the build plate temperature distribution, while the right half simultaneously measures temperatures of surfaces beyond the build plane, including the filament. Fig. 13 plots the measured temperature distribution at multiple times for 3600 mm/min raster speed. As expected, both in-plane temperature distribution (on the left) and filament temperature distribution (on the right) are obtained simultaneously. Note that temperature data for the left and right halves are obtained with separate emissivity calibrations – for graphite and ABS, respectively.

3.6. Calibration

Supplementary Figure S1[1] plots results from calibration experiments

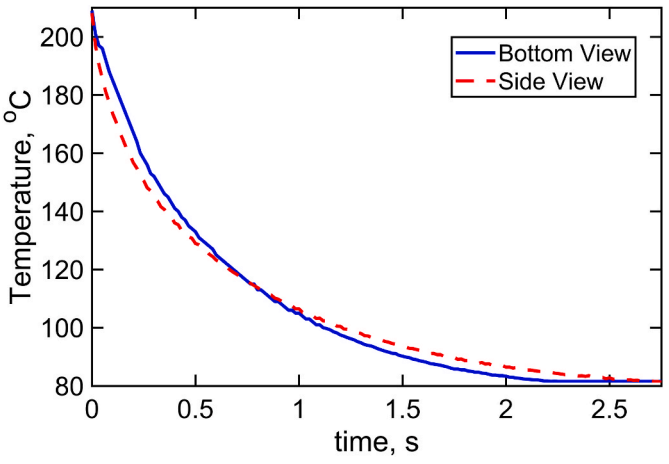

Fig. 12. Comparison of temperature decay with time at a specific point on the filament for bottom-view and side-view measurements.

[1] Supplementary information available on the DOI page of the publication.

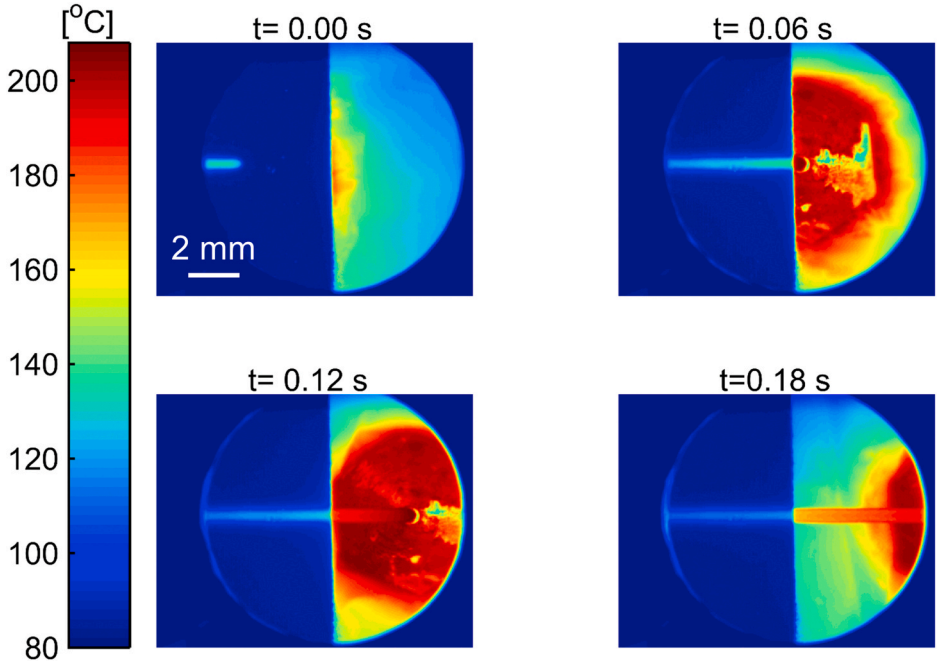

Fig. 13. Measured temperature field when only the left half of the Sapphire window is sprayed with graphite. Colormaps are shown at four different times as the nozzle traverses at 3600 mm/min from left to right.

described in Section 2.2. An emissivity value of 0.806 for the graphite film is found to be result in excellent agreement between the measured temperature and set temperature. Experimental data are linear and very close to the ideal 45° line shown in Supplementary Figure S1. Note that this calibration curve covers and goes beyond the temperature range expected in the actual experiments. A separate calibration experiment carried out for the ABS material resulted in similar data, and is used for experiments that measure the filament temperature.

3.7. Effect of sapphire window

In the present experiments, a portion of the Aluminum bed is replaced with a Sapphire window to enable infrared thermography, which would not be possible with the IR-opaque Aluminum. It is important to estimate the impact of use of the Sapphire window on the temperature field. Experiments are carried out to compare temperature rise during filament dispense on the Sapphire window with that on the Aluminum bed for the same process conditions. Since in-plane infrared thermography on the Aluminum bed is not possible due to the IR-opaque nature of Aluminum, temperature measurement in this comparison experiment is carried out using a thermocouple attached to the Sapphire or Aluminum, over which the filament is dispensed. Measured temperature as a function of time for both cases is presented in Supplementary Figure S2[1]. Supplementary Figure S2 shows that the Sapphire window and Aluminum bed have similar thermal responses to the filament dispensing process. The nature of temperature decay is similar in both cases, although the peak temperature is somewhat different in the two cases. The measured peak temperature for Sapphire is somewhat lower than Aluminum, which may be due to slight differences in the positioning of the thermocouple bead with respect to the rastering filament, both of which are of comparable physical size. Also note that the temperature rise measured is lower than expected for both cases, which is likely because of the relatively large thermal mass of the thermocouple bead in comparison to the size of the rastering filament.

4. Conclusions

It is important to contrast and compare the present method with past work that reported side-view measurements of the temperature field [17,18]. While side-view measurements provide thermal information about inter-layer filament bonding, the present work provides information about intra-layer filament bonding. Both bonding processes are important and contribute towards good thermal and mechanical properties of the printed part. Side-view measurements reported earlier and in-plane measurements reported in this work may be viewed as being complementary – together, they provide a more complete thermal picture of the polymer AM process than just by themselves.

A key limitation of the present work is that bottom-view measurement is limited to printing of the first layer only and its interactions with the build plate. Because bottom-view thermography requires an IR-transparent substrate, the method does not work well for subsequent layers when the view is obscured by the previously deposited layers that are not transparent to IR. In such a case, some thermal information may be obtained using a side-view measurement, although measurements of the temperature between in-plane neighbors will not be possible even with side view measurements.

This work complements previously reported infrared-based temperature measurements of polymer AM processes by measuring the in-plane view of the temperature field instead of the side-view. The additional information obtained through this work helps understand important thermal phenomena, such as in-plane filament-to-filament interface temperature, the extent of in-plane thermal influence of a hot filament, as well as the impact of process parameters such as filament-to-filament gap on such thermal transport phenomena. It is expected that enhanced understanding of filament-to-filament and filament-to-bed adhesion driven by robust temperature field measurements will aid in the printing of parts with novel thermal and mechanical properties.

Data availability statement

The raw/processed data required to reproduce these findings cannot be shared at this time as the data also forms part of an ongoing study.

CRediT authorship contribution statement

Hardikkumar Prajapati: Methodology, Investigation,

Visualization, Data curation, Writing - original draft, Writing - review & editing. **Swapnil S. Salvi:** Investigation, Visualization, Writing - original draft, Writing - review & editing. **Darshan Ravoori:** Investigation, Visualization, Writing - original draft, Writing - review & editing. **Ankur Jain:** Conceptualization, Methodology, Supervision, Project administration, Writing - original draft, Writing - review & editing.

Declaration of competing interest

The authors declare that they have no known competing financial interests or personal relationships that could have appeared to influence the work reported in this paper.

Appendix A. Supplementary data

Supplementary data to this article can be found online at https://doi.org/10.1016/j.polymertesting.2020.106866.

References

[1] D. Dimitrov, K. Schreve, N. de Beer, 'Advances in three dimensional printing – state of the art and future perspectives, Rapid Prototyp. J. 12 (2006) 136–147.

[2] D.T. Pham, R.S. Gault, A comparison of rapid prototyping technologies, Int. J. Mach. Tool Manufact. 38 (1998) 1257–1287.

[3] J.-P. Kruth, M.C. Leu, T. Nakagawa, Progress in additive manufacturing and rapid prototyping, CIRP Ann. - Manuf. Technol. 2 (1998) 525–540.

[4] S. Bose, S. Vahabzadeh, A. Bandyopadhyay, Bone tissue engineering using 3D printing, Mater. Today 12 (2013) 496–504.

[5] D.W. Hutmacher, Scaffolds in tissue engineering bone and cartilage, Biomaterials 21 (2000) 2529–2543.

[6] K.R. Hart, R.M. Dunn, J.M. Sietins, C.M.H. Mock, M.E. Mackay, E.D. Wetzel, Increased fracture toughness of additively manufactured amorphous thermoplastics via thermal annealing, Polymer 144 (2018) 192–204.

[7] D. Ravoori, L. Alba, H. Prajapati, Investigation of process-structure-property relationships in polymer extrusion based additive manufacturing through in situ high speed imaging and thermal conductivity measurements, Addit. Manuf. 23 (2018) 132–139.

[8] H. Prajapati, D. Ravoori, R.L. Woods, A. Jain, Measurement of anisotropic thermal conductivity and inter-layer thermal contact resistance in polymer fused deposition modeling (FDM), Addit. Manuf. 21 (2018) 84–90.

[9] H. Prajapati, D. Chalise, D. Ravoori, R.M. Taylor, A. Jain, Improvement in build-direction thermal conductivity in extrusion-based polymer additive manufacturing through thermal annealing, Addit. Manuf. 26 (2019) 242–249.

[10] C.S. Shafer, D.H. Siddel, A.L. Merriman, A.M. Elliot, Cleated print surface for fused deposition modeling, in: Proceedings of the 27th Annual International Solid Freeform Fabrication Symposium, 2016, pp. 1359–1365.

[11] S.F. Costa, F.M. Duarte, J.A. Covas, Estimation of filament temperature and adhesion development in fused deposition techniques, J. Mater. Process. Technol. 245 (2017) 167–179.

[12] C. Bellehumeur, L. Li, Q. Sun, P. Gu, Modeling of bond formation between polymer filaments in the fused deposition modeling process, J. Manuf. Process. 6 (2004) 170–178.

[13] J.E. Seppala, S. Hoon Han, K.E. Hillgartner, C.S. Davis, K.B. Migler, Weld formation during material extrusion additive manufacturing, Soft Matter 13 (38) (2017) 6761–6769.

[14] M. Spoerk, J. Gonzalez-Gutierrez, J. Sapkota, S. Schuschnigg, C. Holzer, Effect of the printing bed temperature on the adhesion of parts produced by fused filament fabrication, Plast. Rubber Compos. 47 (1) (2018) 17–24. Jan.

[15] F. Yang, R. Pitchumani, Healing of thermoplastic polymers at an interface under nonisothermal conditions, Macromolecules 35 (8) (2002) 3213–3224.

[16] Q. Sun, G.M. Rizvi, C.T. Bellehumeur, P. Gu, Effect of processing conditions on the bonding quality of FDM polymer filaments, J. Manuf. Process. 14 (2008) 72–80.

[17] D. Ravoori, C. Lowery, H. Prajapati, A. Jain, Experimental and theoretical investigation of heat transfer in platform bed during polymer extrusion based additive manufacturing, Polym. Test. 73 (2019) 439–446.

[18] J.E. Seppala, K.D. Migler, Infrared thermography of welding zones produced by polymer extrusion additive manufacturing, Addit. Manuf. 12 (2016) 71–76.

[19] K. Choo, et al., Heat retention modeling of large area additive manufacturing, Addit. Manuf. 28 (2019) 325–332.

[20] J. Go, A.J. Hart, Fast desktop-scale extrusion additive manufacturing, Addit. Manuf. 18 (2017) 276–284. Dec.

[21] D.D. Phan, Z.R. Swain, M.E. Mackay, Rheological and heat transfer effects in fused filament fabrication, J. Rheol. 62 (5) (2018) 1097–1107.

[22] H. Prajapati, D. Ravoori, A. Jain, Measurement and modeling of filament temperature distribution in the standoff gap between nozzle and bed in polymer-based additive manufacturing, Addit. Manuf. 24 (2018) 224–231. Dec.

[23] M. Vollmer, K.-P. Möllmann, Infrared Thermal Imaging: Fundamentals, Research and Applications, second ed., Wiley-VCH Verlag, 2017, ISBN 9783527413515.

[24] D. Ravoori, H. Prajapati, V. Talluru, A. Adnan, A. Jain, Nozzle-integrated pre-deposition and post-deposition heating of previously deposited layers in polymer extrusion based additive manufacturing, Addit. Manuf. 28 (2019) 719–726.

[25] C.B. Sweeney, et al., "Welding of 3D-printed carbon nanotube–polymer composites by locally induced microwave heating, Sci. Adv. 3 (2017), e1700262.

[26] A. Nycz, V. Kishore, J. Lindahl, C. Duty, C. Carnal, V. Kunc, Controlling substrate temperature with infrared heating to improve mechanical properties of large-scale printed parts, Addit. Manuf. 33 (2020) 101068. May.

[27] R.B. Dinwiddie, et al., Infrared imaging of the polymer 3D-printing process, in: Thermosense: Thermal Infrared Applications XXXVI, 2014, p. 910502.

[28] X. Zhou, S.-J. Hsieh, Thermal analysis of fused deposition modeling process using infrared thermography imaging and finite element modeling, in: Thermosense: Thermal Infrared Applications XXXIX, 2017, p. 1021409.

[29] E. Malekipour, S. Attoye, H. El-Mounayri, Investigation of Layer Based Thermal Behavior in Fused Deposition Modeling Process by Infrared Thermography, in: Procedia Manufacturing, 2018.